

Primordial Black Holes and Gravitational Waves in Hybrid Inflation with Chaotic Potentials

Waqas Ahmed^{a 1}, M. Junaid^{b 2} and Umer Zubair^{c,d 3}

^a *School of Mathematics and Physics, Hubei Polytechnic University,
Huangshi 435003, China*

^b *National Centre for Physics, Islamabad, Pakistan*

^c *Department of Physics and Astronomy,
University of Delaware, Newark, DE 19716, USA*

^d *College of Humanities and Sciences, Thomas Jefferson University,
East Falls Campus, Philadelphia, PA 19144, USA*

Abstract

We study the formation of primordial black hole (PBH) dark matter and the generation of scalar induced secondary gravitational waves (SIGWs) in a non-supersymmetric model of hybrid inflation with chaotic (polynomial-like) potential, including one-loop radiative corrections. A radiatively corrected version of these models is entirely consistent with Planck's data. By adding non-canonical kinetic energy term in the lagrangian, the inflaton experiences a period of ultra-slow-roll, and the amplitude of primordial power spectrum is enhanced to $O(10^{-2})$. The enhanced power spectra of primordial curvature perturbations can have both sharp and broad peaks. A wide mass range of PBH is realized in our models, and the frequencies of scalar induced gravitational waves are ranged from nHz to Hz. We present several benchmark points where the PBH mass generated during inflation is around $(1 - 100) M_{\odot}$, $(10^{-9} - 10^{-7}) M_{\odot}$ and $(10^{-16} - 10^{-11}) M_{\odot}$. The PBHs can make up most of the dark matter with masses around $(10^{-16} - 10^{-11}) M_{\odot}$ and $(1 - 100) M_{\odot}$, and their associated SIGWs can be probed by the upcoming space-based gravitational wave (GW) observatories. The formation of $10 M_{\odot}$ PBH with wide peaks of SIGWs can be used to interpret the stochastic GW signal in the nHz band, detected by the North American Nano hertz Observatory (NANO-Grav) for Gravitational Waves. These signals may also be tested by future interferometer-type GW observations of EPTA, SKA, LISA, TaiJi, TianQin and Einstein Telescope (ET).

¹E-mail: waqasmit@hbpu.edu.cn

²E-mail: mjunaid@ualberta.ca

³E-mail: umer@udel.edu

1 Introduction

From astronomical and cosmological observations, there is convincing evidence that 85% of the matter in the Universe is in the form of cold, non-baryonic dark matter (DM)[1]. The study of Primordial Black Holes (PBHs) dates back to the 1960's and 70's[2, 3, 4], and shows that the PBHs may form due the collapse of large overdensities during early universe. The early universe may contain regions with high densities at small scales that can trigger gravitational collapse to form PBH. This PBH production can be tested through their effects on a variety of cosmological and astronomical processes, and therefore, can serve as an inspiring tool to probe physics in the very early Universe [5, 6]. In particular, PBH could be a potential candidate for (a fraction of) dark matter (DM), which has drawn a lot of attention [7, 8].

PBHs are non-baryonic, as they form before matter-radiation equality. The PBHs with masses $\lesssim 10^{15}$ g would have evaporated by now emitting Hawking radiation [9]. The emitted particles may impact the gamma-ray background [10] and the abundance of light elements produced by the big bang nucleosynthesis [11]. The PBHs with masses greater than 10^{15} g, on the other hand may survive up to the present epoch and are expected to be constrained by their gravitational effects, such as gravitational lensing [12], dynamical effects on baryonic matter [13], or the fast radio bursts created by mergers of charged PBHs [14].

The Laser Interferometer Gravitational-Wave Observatory (LIGO), the Scientific Collaboration and the Virgo Collaboration have detected several events of GWs coming from the merger of black holes (BHs) [15, 16, 17, 18, 19]. Recently, the North American Nano hertz Observatory for Gravitational Wave (NANO-Grav) Collaboration [20] has published an analysis of the 12.5 yrs pulsar timing array (PTA) data, where strong evidence of a stochastic process with a common amplitude and a common spectral slope across pulsars was found. These two observations moved the physicists attention toward the gravitational waves (GWs) generated by PBH-PBH mergers [21, 22, 23], as well as the scalar-induced GWs from the enhanced primordial density perturbations associated with PBH formation [24, 25, 26, 27, 28, 29]. The GWs survey shall be a promising window to reveal the physical processes of PBH formations.

The scalar induced gravitational waves (SIGWs) associated with the formation of PBHs may be the source of the NANO-Grav signal [30], or the GWs detected by LIGO-Virgo. Therefore, the formation of PBHs can be observed by future interferometer based experiments such as the LIGO-Virgo and the pulsar timing signals of NANO-Grav. In order to produce PBH in the radiation era from the gravitational collapse of overdense regions, it is required that the density of overdense regions exceed the threshold value at the horizon re-entry. The initial conditions for these overdense regions are produced during the inflationary era. To produce the desired abundance of PBHs one needs the primordial scalar power spectrum at small scales to be enhanced to $P_{\zeta}(k > 1) \sim O(0.01)$. This condition is also required to explain the NANO-Grav signal if it is regarded as a SIGW. On the other hand, the constraint

on the amplitude of power spectrum at large scales from the cosmic microwave background (CMB) anisotropy measurements from [31] is $P_\zeta(0.05) \sim O(10^{-9})$. To produce enough abundance of PBH dark matter (DM) and signals measurable by Nano-Grav, the amplitude of the power spectrum at small scales should be enhanced at least seven orders of magnitude to reach the threshold value.

In this paper, we study the non-supersymmetric model of Hybrid inflation and the formation of primordial black hole (PBH) dark matter along with the generation of scalar induces secondary gravitational waves (SIGWs). In order to produce the required abundance of PBHs, we enhance the power spectrum using the mechanism discussed in [32]. This mechanism relies on the incorporation of a non-canonical kinetic term with a function $G(\phi)$ which exhibits a peak at some value of the field ϕ_p . Beyond this point, $G(\phi)$ falls exponentially, suppressing the scalar perturbations to the value observed today. Several other enhancement mechanisms are also discussed in the literature as well. Ref [33] the enhancement by ultra-slow-roll inflation with an inflection point. The other possibility is fine-tuning the model parameters while keeping the total number of e-folds around 50-60 [34]. After the formation of PBHs, the power spectrum enhancement at small scales induces secondary SIGWs after the horizon reentry during the radiation-dominated epoch [35]. These SIGWs have a vast range of frequencies and consist of a stochastic background that can be detected by pulsar timing arrays (PTA), the space-based GW detectors such as Laser Interferometer Space Antenna(LISA), Taiji, and TianQin [36, 37, 38, 39], that will help disclose the properties of PBHs and primordial power spectrum at small scales.

The layout of the paper is as follows. In Sec.2 we describe the basic features of the model. The inflation and PBHs production is described in Sec.3. In sections 4 and 5 we discuss PBH abundance and Production of SIGWs with numerical analysis. Our conclusions are summarized in Sec.6.

2 Description of the Model

The scalar potential of hybrid inflation (HI) can be expressed as a combination of Higgs potential $V(\chi)$ and inflaton potential $\delta V(\phi)$ with an additional term, $g^2\chi^2\phi^2$, that represents the interaction between the Higgs field χ and inflaton ϕ . The tree-level hybrid inflation (TLHI) potential, therefore, can be written as

$$V(\chi, \phi) = \kappa^2 \left(M^2 - \frac{\chi^2}{4} \right)^2 + \frac{g^2\chi^2\phi^2}{4} + \delta V(\phi), \quad (1)$$

where $\delta V(\phi)$, the inflaton potential, is taken to be a chaotic polynomial-like potential, i.e., $\delta V(\phi) = \lambda_p\phi^p$ with $p > 0$. Here, the role of the interaction term is to generate an effective (squared) mass,

$$m_\chi^2 = -\kappa^2 M^2 + \frac{g^2\phi^2}{2} = \frac{g^2}{2} (\phi^2 - \phi_c^2), \quad \text{with } \phi_c \equiv \frac{\sqrt{2}\kappa M}{g}, \quad (2)$$

for the χ field in the $\chi = 0$ direction. This direction is a local minimum for $\phi > \phi_c = \frac{\sqrt{2}\kappa M}{g}$ and can be used for inflation with effective single field potential given by

$$V(\phi) = \kappa^2 M^4 + \delta V(\phi) = V_0 + \lambda_p \phi^p, \quad (3)$$

where $V_0 = \kappa^2 M^4$. The chaotic potential, here, provides the necessary slope for the slow-roll inflation in the otherwise flat-valley. We consider suitable initial conditions for inflation to occur only in the $\chi = 0$ valley until $\phi = \phi_c$ is reached where inflation is terminated abruptly, followed by a waterfall phase transition.

We now tend to include one-loop radiative corrections, as the tree level predictions are not consistent with the Planck 2018 results [40]. The radiative corrections arise from the possible couplings of inflaton with other fields. These couplings can contribute to the reheating process in order to recover the hot big bang initial conditions. The corrections arising from the coupling of inflaton to fermions or bosons may be termed as fermionic or bosonic radiative corrections. The one-loop radiative corrections to $V(\phi)$ in the inflationary valley can be found from the following form of Coleman-Weinberg formula [41],

$$V_{1\text{-loop}} = A \phi^4 \ln \left(\frac{\phi}{\phi_c} \right), \quad (4)$$

where $A < 0$ ($A > 0$) for fermionic (bosonic) radiative corrections. The fermionic radiative corrections have already been seen to play an important role for the chaotic inflation driven by the quadratic and the quartic potentials [42]. The fermionic radiative corrections generally reduce both r and n_s in the chaotic inflation. Therefore, in rest of the paper we study the effect of fermionic radiative corrections on the tree-level predictions and compare them with the Planck's latest bounds on r and n_s .

Using Eqs.(3) and (4), the one-loop radiatively corrected hybrid inflationary (RCHI) potential can be written as,

$$V = V_0 + \lambda_p \phi^p - A \phi^4 \ln \left(\frac{\phi}{\phi_c} \right). \quad (5)$$

In order to discuss the predictions of the model, some discussion of the effective number of independent parameters is in order. Apart from the λ_p parameter of the chaotic potential, the fundamental parameters of the potential in Eq. (1) are κ , g and M , which can be reduced to V_0 and ϕ_c for the effective potential in Eq. (3). We, however, take V_0 and $\kappa_c \equiv g^2/\kappa$ as the effective independent parameters with $\phi_c = \sqrt{2V_0^{1/2}/\kappa_c}$. With this choice we can develop a simple correspondence for the supersymmetric hybrid inflation for which $\kappa_c = g = \kappa$ [43].

Model	V_0	λ_p	A	ϕ_c	ϕ_*	n_s	r
p=2/3	5.45×10^{-11}	1.31×10^{-12}	2.96×10^{-14}	0.1215	0.788	0.965	0.0018
p=1	5.45×10^{-11}	9.76×10^{-13}	8.79×10^{-14}	0.1215	0.63	0.965	0.00176
p=2	5.45×10^{-11}	9.33×10^{-13}	1.67×10^{-13}	0.1215	0.76	0.965	0.00173

Table 1: Hybrid inflation with chaotic potential parameters V_0 , λ_p , A and ϕ_c for three polynomials $p = 2/3$, $p = 1$ and $p = 2$. ϕ_* corresponds to the value of ϕ at the pivot scale $k_* = 0.05 \text{ Mpc}^{-1}$. The scalar spectral index n_s and power spectra $P_\zeta(k_*) = 2.15 \times 10^{-9}$ are evaluated at the pivot scale k_* for the three chaotic potentials.

3 Inflation and PBHs Production

PBHs are formed from the gravitational collapse of over-dense regions with their density contrasts at the horizon reentry during radiation domination exceeding the threshold value. The overdense regions may be seeded from the primordial curvature perturbations generated during inflation. The feasible way to produce enough abundance of PBH DM is by enhancing the amplitude of the power spectrum at least seven orders of magnitude to reach the threshold at small scales. We are using the enhancement mechanism of the power spectrum at small scales proposed in Refs [32] using Kinetic or K/G Inflation. The Kinetic inflation is defined when Inflaton field's kinetic part is coupled to Inflaton field function $K(\phi) = 1 + G(\phi)$ as [44]

$$S = \int d^4x \sqrt{-g} \left(m_p^2 \frac{R}{2} - \frac{1}{2} g^{\mu\nu} K(\phi) \partial_\mu \phi \partial_\nu \phi + V(\phi) \right),$$

where $m_p = 1/\sqrt{8\pi G} = 1$. The background equations of motion are

$$H^2 = \frac{1}{3} \left(K(\phi) \frac{\dot{\phi}^2}{2} + V(\phi) \right), \quad (6)$$

$$\dot{H} = -K(\phi) \frac{\dot{\phi}^2}{2}, \quad (7)$$

$$\ddot{\phi} = -3H\dot{\phi} - \frac{V_{,\phi} + K_{,\phi} \dot{\phi}^2/2}{K(\phi)}, \quad (8)$$

where $K_{,\phi} = dK(\phi)/d\phi$. Now, one can convert these equations into number of e-folds $n = \ln(a)$ as follows

$$H^2 = \frac{2V}{6 - K(\phi)\phi_{,n}^2}, \quad (9)$$

$$H_{,n} = -K(\phi)H \frac{\phi_{,n}^2}{2}, \quad (10)$$

$$\phi_{,nn} = - \left(3 + \frac{H_{,n}}{H} \right) \left(\phi_{,n} + \frac{V_{,\phi}}{K(\phi)V} \right) - \frac{\phi_{,n}^2 K_{,\phi}}{2K(\phi)}. \quad (11)$$

The slow-roll parameters are defined as

$$\epsilon_1 = -\frac{\dot{H}}{H^2} = -\frac{H_{,n}}{H}, \quad (12)$$

$$\epsilon_2 = -\frac{\ddot{\phi}}{H\dot{\phi}} = -\left(\frac{\phi_{,nn}}{\phi_{,n}} + \frac{H_{,n}}{H}\right), \quad (13)$$

$$\epsilon_K = \frac{\dot{\phi}K_{,\phi}}{HK(\phi)} = \frac{\phi_{,n}K_{,\phi}}{K(\phi)}, \quad (14)$$

where last slow roll parameter is specific for Kinetic Inflation. The slow-roll inflation is realized when $|\epsilon_i| \ll 1$, where $i = 1, 2, K$.

The second order action $S^{(2)}$ in perturbation theory of the curvature perturbation ζ , for Kinetic Inflation is [45],

$$S^{(2)} = \frac{1}{2} \int d\tau d^3x \tilde{z}^2 K(\phi) [(\zeta')^2 - (\vec{\nabla}\zeta)^2], \quad (15)$$

where $\tilde{z} = a(t)\dot{\phi}/H$ and $K(\phi) = 1 + G(\phi)$. $a(t)$ represents the scale factor, $c_s^2 = K(\phi)$ is the speed of sound and the prime in ζ' represents derivative with respect to the conformal time $\tau = \int dt/a(t)$. Using $z = \sqrt{K}\tilde{z}$ in the quadratic action in Eq. (15) and varying with the respect to curvature perturbation $\zeta_k = v_k/z$ and v_k in the Fourier space, we obtain the famous Mukhanov equations for scalar perturbations

$$v_k'' + \left(k^2 - \frac{z''}{z}\right)v_k = 0, \quad (16)$$

$$\zeta_k'' + 2\frac{z'}{z}\zeta_k' + k^2\zeta_k = 0. \quad (17)$$

We can again convert the above mode equation for ζ_k to the number of e-folds n as follows

$$\zeta_{k,nn} + \left(3 + \frac{H_{,n}}{H} + \frac{2\phi_{,nn}}{\phi_{,n}} + \frac{\phi_{,n}K_{,\phi}}{K(\phi)}\right)\zeta_{k,n} + \left(\frac{k}{aH}\right)^2 \zeta_k = 0, \quad (18)$$

$$\zeta_{k,nn} + (3 + \epsilon_1 - 2\epsilon_2 + \epsilon_K)\zeta_{k,n} + \left(\frac{k}{aH}\right)^2 \zeta_k = 0. \quad (19)$$

In the above expressions for mode equation we have used $z = \sqrt{K(\phi)}a\phi_{,n}$ and $\frac{z'}{z} = aH\left(1 + \frac{\phi_{,nn}}{\phi_{,n}} + \frac{\phi_{,n}K_{,\phi}}{2K(\phi)}\right)$. Numerically it is more convenient to solve the equation for ζ_k rather than standard Mukhanov variable v_k as ζ_k gives stable results.

Solving the mode Eq. (17) with Bunch Davies vacuum[46], we obtain the scalar power spectrum on super horizon scales $|k\tau| \ll 1$,

$$P_\zeta(k) = \frac{k^3|\zeta_k|^2}{2\pi^2m_p^2} = \frac{H_*^2}{8\pi^2m_p^2\epsilon_1^*}, \quad (20)$$

where $*$ marks the horizon crossing values for each mode k . The scalar spectral index and tensor to scalar ratio r for KG-Inflation at the pivot scale is given by

$$n_s = 1 + \frac{1}{K} \left(2\eta_V - 6\epsilon_V - \sqrt{2\epsilon_V} \frac{K_{,\phi}}{K} \right), \quad (21)$$

$$r = \frac{P_T}{P_\zeta} \simeq 16\epsilon_V/K, \quad (22)$$

$$N = \int_{\phi_e}^{\phi_*} \frac{d\phi}{\sqrt{2\epsilon_1}} \simeq \int_{\phi_e}^{\phi_*} d\phi \frac{\sqrt{KV}}{V_{,\phi}}, \quad (23)$$

where $\epsilon_V = (V_{,\phi}/V)^2/2$, $\eta_V = V_{,\phi\phi}/V$ and N is the total number of e-folds.

Model, $K_{g/s}$	h	w	ϕ_p	Ω_{GW}^{peak}
p=2/3, K_g	2.0×10^3	2.0×10^{-4}	0.3	6.57×10^{-10}
p=1, K_g	2.0×10^3	1.7×10^{-4}	0.3	8.93×10^{-10}
p=2, K_g	1.8×10^3	1.7×10^{-4}	0.2	2.19×10^{-9}
p=2/3, K_s	2.0×10^3	6.06×10^{-3}	0.3	6.57×10^{-10}
p=1, K_s	2.0×10^3	5.6×10^{-3}	0.3	9.08×10^{-10}
p=2, K_s	1.5×10^3	4.5×10^{-3}	0.21	9.43×10^{-10}

Table 2: Data points for hybrid inflation potential with $p = 2/3$, $p = 1$ and $p = 2$ using Gaussian peak function $K_g(\phi)$ and the step function $K_s(\phi)$.

The CMB power spectrum as reported by Planck 2018 [31] at the pivot scale $k^* = 0.05 \text{ Mpc}^{-1}$ is $P_\zeta(k^*) = 2.15 \times 10^{-9}$. For the production of PBHs, one needs to enhance the power spectrum to $P_\zeta(k) \approx 10^{-2}$ at small scales $k > 10^2 \text{ Mpc}^{-1}$. This enhancement in the power spectrum can be achieved using $K(\phi) = 1 + G(\phi)$, as some kind of peak functions. For instance, one can have a Gaussian peak function $K_g(\phi)$, a polynomial power function $K_q(\phi)$, as discussed in [32], and a step function $K_s(\phi)$,

$$K_g(\phi) = 1 + h e^{-\frac{(\phi-\phi_p)^2}{2w^2}}, \quad (24)$$

$$K_q(\phi) = 1 + \frac{h}{\sqrt[q]{1 + \frac{|\phi-\phi_p|^q}{w^q}}}, \quad (25)$$

$$K_s(\phi) = 1 + \begin{cases} h & \phi_p - w/2 < \phi < \phi_p + w/2 \\ 0 & \phi > \phi_p + w/2, \phi < \phi_p - w/2 \end{cases}. \quad (26)$$

These peak functions are plotted in Fig. 1 as a function of ϕ . It can be seen that the polynomial peak functions $K_{q=1,2}$ have wider base and falls off slowly. The Gaussian peak function K_g falls off exponentially with a narrow base whereas, the step peak function K_s has a flat top with the width exactly equal to w . Due to this peak

function, the first slow roll parameter ϵ becomes very small, of the order of 10^{-10} . This leads to ultra slow-roll inflation; the inflaton field gets trapped in this local minimum for 25 to 40 efolds as can be seen in Fig. 2. Because of inverse relation between the power spectrum P_ζ and ϵ , the sudden fall in the value of ϵ enhances the scalar power spectrum P_ζ by seven order of magnitude. This enhancement in power spectra can be realized in String theory-inspired inflation models due to large parametric space and the possibility of colliding branes. [47]

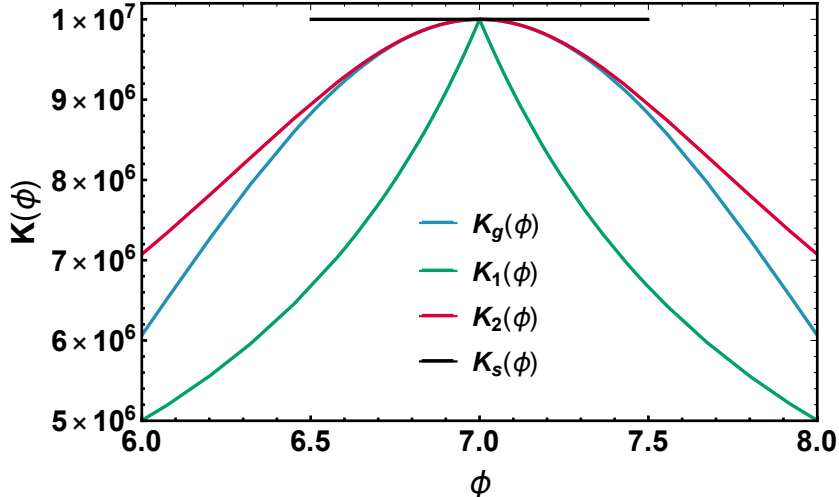


Figure 1: Gaussian peak function $K_g(\phi)$, polynomial power function $K_q(\phi)$, with $q = 1, 2$, and a step function $K_s(\phi)$ as a function of ϕ for $h = 10^7$ and $w = 1$.

We will calculate different cosmological observables such as, power spectrum $P_\zeta(k)$, fraction of GWs $\Omega_{GW}(f)$ and PBH abundance Y_{pbh} using different peak functions. We ensure that the total number of efolds vary between 56 to 64, enough to solve the horizon problem. The parameters h , w and ϕ_p for different peak functions used here are given in Tables 2 and 3.

The scalar power spectrum $P_\zeta(k)$ is plotted in Fig. 3 for our hybrid inflation model described by the scalar potential in Eq. (5). Here, we have employed the functions $K_g(\phi)$, $K_q(\phi)$ and $K_s(\phi)$, defined in Eqs. (24), (25) and (26), to enhance the power spectrum. The top left, top right and middle left panels of Fig. 3, are plotted using the polynomial peak function $K_q(\phi)$ with $q = 2$ for $p = 2/3$, $p = 1$ and $p = 2$, respectively. The three curves correspond to the data points for NG (blue), TL (black) and ET (red) from Table 3. It is clear from these plots that the power spectra at CMB scales is well within the Planck bounds, while at shorter scales ($k > 10 \text{ Mpc}^{-1}$) the $P_\zeta(k)$ peaks are of the order of 10^{-2} to produce PBHs.

The middle right, bottom left and bottom right panels in Fig. 3 are plotted for $p = 2/3$, $p = 1$ and $p = 2$, respectively using the Gaussian peak function $K_g(\phi)$ (black curves) and the step peak function $K_s(\phi)$ (blue curves). It can be seen that these curves lie at the border of μ -distortion region as we calibrated the data points carefully in table 2.

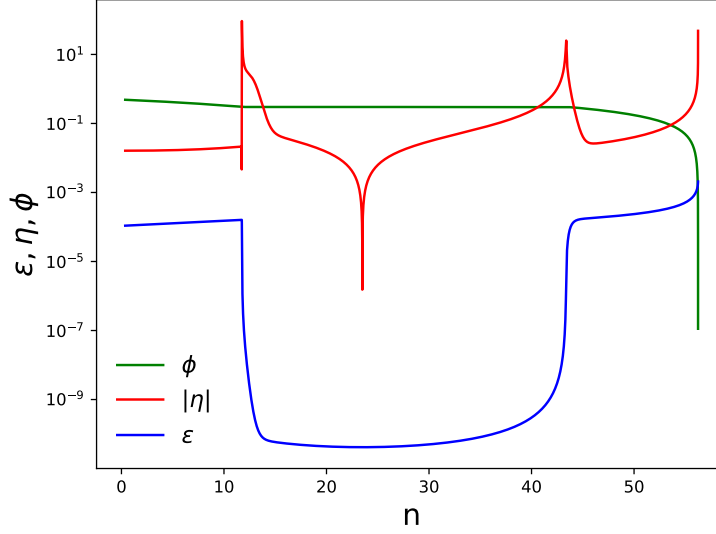


Figure 2: Behavior of background parameters ϕ , ϵ and $|\eta|$ with respect to the number of e -folds $n = \log(a)$. The curves are plotted using the Gaussian peak function $K_g(\phi)$. The numerical values of the relevant parameters are given in Table 2.

Detector, Model	h	w	ϕ_p	Y_{pbh}^{peak}	Ω_{GW}^{peak}
NG, $p=2/3$	9.3×10^9	$1. \times 10^{-12}$	0.725	3.15×10^{-31}	9.85×10^{-10}
TL, $p=2/3$	10.526×10^9	1.0×10^{-12}	0.595	0.105	1.31×10^{-8}
ET, $p=2/3$	12.01×10^9	1.0×10^{-12}	0.465	0.65	1.1×10^{-8}
SE, $p=2/3$	9.67×10^9	1.0×10^{-12}	0.696	0.167	2.34×10^{-8}
NG, $p=1$	9.1×10^9	1.0×10^{-12}	0.565	1.5×10^{-45}	5.27×10^{-10}
TL, $p=1$	10.177×10^9	1.0×10^{-12}	0.4	0.006	8.75×10^{-9}
ET, $p=1$	10.376×10^9	1.0×10^{-12}	0.23	0.809	6.13×10^{-9}
SE, $p=1$	9.59×10^9	1.0×10^{-12}	0.53	0.177	2.15×10^{-8}
NG, $p=2$	6.73×10^8	1.35×10^{-11}	0.63	4.4×10^{-45}	7.37×10^{-10}
TL, $p=2$	6.599×10^8	1.2×10^{-11}	0.45	0.0029	7.76×10^{-9}
ET, $p=2$	7.346×10^8	1.0×10^{-11}	0.40	0.812	1.14×10^{-8}
SE, $p=2$	6.944×10^8	1.35×10^{-11}	0.63	0.022	2.19×10^{-8}

Table 3: Data points for hybrid inflation potential with $p = 2/3$, $p = 1$ and $p = 2$ using polynomial peak function $K_{q=2}(\phi)$. The labels NG, TL, ET and SE corresponds to peaks location of GW fraction $\Omega_{GW}(f)$ curve in regions of Detectors; NANO-Grav (NG), TaiJi/Lisa (TL), Einstein Telescope (ET) and SKA/EPTA (SE), respectively.

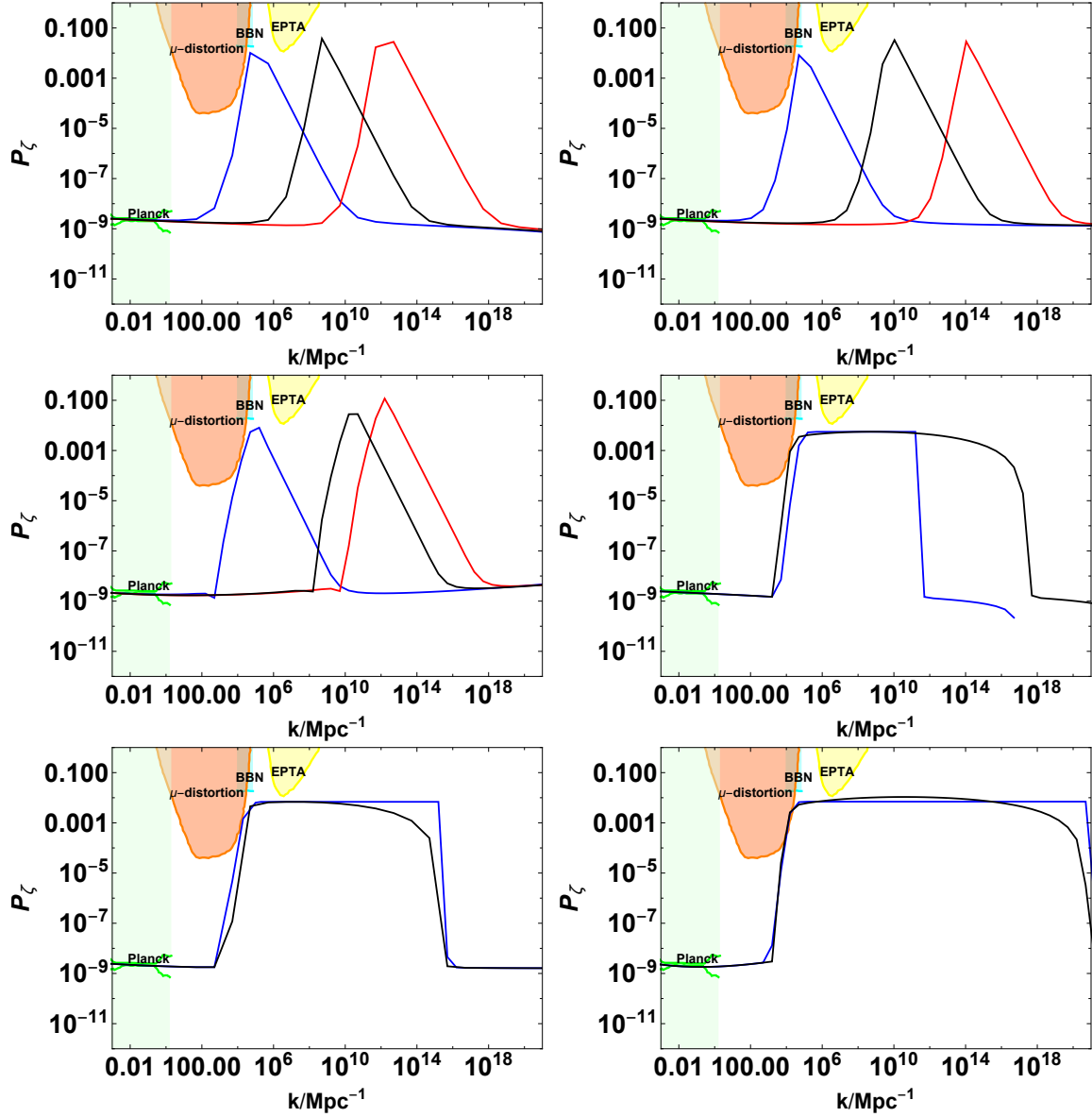


Figure 3: The scalar power spectrum $P_\zeta(k)$ plotted as a function of scale k using the enhancement functions $K_g(\phi)$, $K_q(\phi)$ and $K_s(\phi)$. The upper left, upper right and middle left panels are respectively drawn for $p = 2/3$, $p = 1$ and $p = 2$ using the polynomial peak function K_q with $q = 2$. The middle right, bottom left and bottom right panels are drawn using the Gaussian peak function K_g (black curves) and the step peak function K_s (blue curves) for $p = 2/3$, $p = 1$ and $p = 2$, respectively.

4 PBH Abundance

When the primordial curvature perturbation re-enters the horizon during radiation dominated era, it may gravitationally collapse to form PBHs. The PBH mass is equal to γM_{hor} , where M_{hor} is the horizon mass and we choose the factor $\gamma = 0.2$ [48]. The current fractional energy density of PBHs with mass M to DM is [7]

$$Y_{\text{PBH}}(M) = \frac{\beta(M)}{3.94 \times 10^{-9}} \left(\frac{\gamma}{0.2}\right)^{1/2} \left(\frac{g_*}{10.75}\right)^{-1/4} \times \left(\frac{0.12}{\Omega_{\text{DM}} h^2}\right) \left(\frac{M}{M_{\odot}}\right)^{-1/2}, \quad (27)$$

where M_{\odot} is the solar mass, g_* are the effective degrees of freedom at the formation time and Ω_{DM} is the current energy density parameter of DM. The fractional energy density of PBHs at the formation is [49, 50]

$$\beta(M) \approx \sqrt{\frac{2}{\pi}} \frac{\sigma(M)}{\delta_c} \exp\left(-\frac{\delta_c^2}{2\sigma^2(M)}\right), \quad (28)$$

where δ_c is the critical density perturbation for the PBH formation and $\sigma(k)$ is the mass variance associated with the PBH mass $M(k)$ smoothing on the co-moving horizon length $k^{-1} = 1/(aH)$, given by [49]

$$\sigma^2(k) = \left(\frac{4}{9}\right)^2 \int \frac{dq}{q} W^2(q/k) (q/k)^4 P_{\zeta}(q), \quad (29)$$

with the Gaussian window function $W(x) = \exp(-x^2/2)$. The effective degrees of freedom

$$g_* = \begin{cases} 10.75 & 0.5\text{MeV} < T < 300\text{GeV} \\ 107.5 & T > 300\text{GeV} \end{cases}. \quad (30)$$

We take the observational value $\Omega_{\text{DM}} h^2 = 0.12$ [51] and $\delta_c = 0.4$ [50, 52] for the calculation of PBH abundance. The relation between the PBH mass M and the scale k is [49]

$$M(k) = 3.68 \left(\frac{\gamma}{0.2}\right) \left(\frac{g_*}{10.75}\right)^{-1/6} \left(\frac{k}{10^6 \text{Mpc}^{-1}}\right)^{-2} M_{\odot}. \quad (31)$$

With the approximation that the power spectrum is scale invariant, we obtain

$$\sigma(k) \simeq (4/9) \sqrt{P_{\zeta}}, \quad (32)$$

$$\beta(M) \approx \sqrt{\frac{2}{\pi}} \frac{\sqrt{P_{\zeta}}}{\mu_c} \exp\left(-\frac{\mu_c^2}{2P_{\zeta}}\right), \quad (33)$$

where $\mu_c = 9\delta_c/4$. Substituting the obtained power spectrum into Eqs. (27), (28), (29) and (31), we obtain the PBH abundances as displayed in Fig. 4 with the parameter sets ET, TL and SE of Table 3. The SE data set corresponds to PBH mass range of

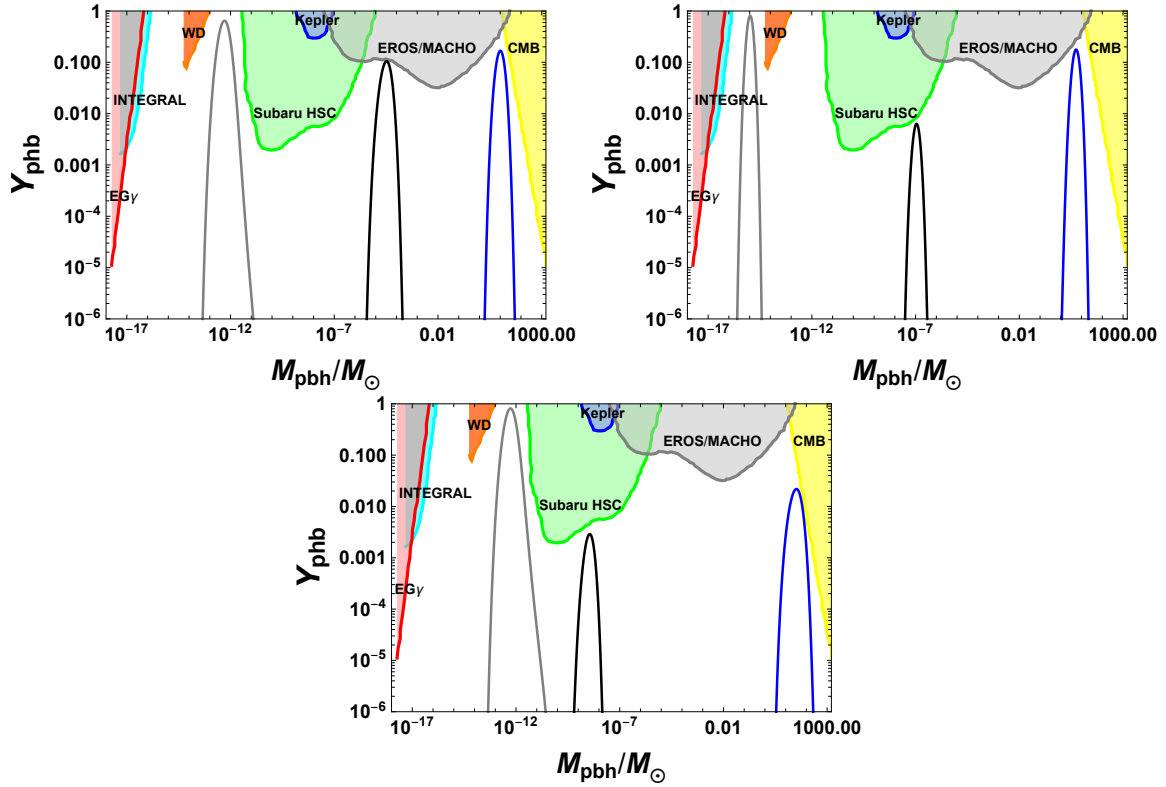


Figure 4: Primordial Black Hole (PBH) abundance Y_{pbh} plotted against the primordial black hole mass M_{pbh}/M_{\odot} for the scalar potential in Eq (5) with $p = 2/3$ (top left), $p = 1$ (top right) and $p = 2$ (bottom). The power spectrum P_{ζ} is calculated using the enhancement mechanism of polynomial peak function $K_q(\phi)$ with $q = 2$. The three peaks in each plot are drawn for the data points ET (gray), TL (black) and SE (blue) from Table 3.

$(1-10) M_{\odot}$ with peaks around $Y_{pbh} \approx 0.16$, which implies that it consists of 16 percent of Dark Matter (DM). The TL points have mass range of $(10^{-8} - 10^{-4}) M_{\odot}$ and peaks around $Y_{pbh} \approx (0.003, 0.10)$ whereas, ET data points have a range $(10^{-16} - 10^{-11}) M_{\odot}$ with $Y_{pbh} \approx (0.133, 0.80)$ that amount to more than 60 to 80 percent of DM.

5 Production of Secondary Gravitational Waves

The production of primordial black holes (PBHs) due to large curvature or density perturbations can induce secondary GWs due to second order mode coupling. These Secondary Induced GW (SIGW) are gauge invariant [30] stochastic background waves that could be observed by future GW experiments.

The tensor mode h_k for SIGW is sourced by quadratic scalar perturbations function $S_k(\Phi_k)$ [25, 24]

$$h_k'' + 2\mathcal{H}h_k' + k^2 h_k = 4S_k(\Phi_k), \quad (34)$$

$$S_k(\Phi_k) = \int \frac{d^3q}{(2\pi)^{\frac{3}{2}}} q^i q^j e_{ij}(k) \left(2\Phi_q \Phi_{k-q} + \frac{4(\Phi_q' + \mathcal{H}\Phi_q)}{3(1+w)\mathcal{H}^2} (\Phi_{k-q}' + \mathcal{H}\Phi_{k-q}) \right), \quad (35)$$

where $\mathcal{H} = aH$, $w = p/\rho$, $e_{ij}(k)$ is polarization tensor and Φ_k is the gauge invariant Bardeen potential[53]. During the radiation dominated era, these SIGWs decouple from their scalar part and plateau after horizon crossing. The energy density of these SIGWs today is given by [30, 54]

$$\begin{aligned} \Omega_{GW}(k) &= 0.387 \frac{\Omega_r}{6} \left(\frac{g_{*,s}^4 g_*^{-3}}{106.75} \right)^{-\frac{1}{3}} \int_{-1}^1 dx \int_1^\infty dy P_\zeta \left(k \frac{y-x}{2} \right) P_\zeta \left(k \frac{x+y}{2} \right) F(x, y) \\ F(x, y) &= \frac{288(x^2 + y^2 - 6)^2 (x^2 - 1)^2 (y^2 - 1)^2}{(x-y)^8 (x+y)^8} \\ &\times \left[\left(x^2 - y^2 + \frac{x^2 + y^2 - 6}{2} \log \left| \frac{y^2 - 3}{x^2 - 3} \right| \right)^2 + \frac{\pi^2}{4} (x^2 + y^2 - 6)^2 \theta(y - \sqrt{3}) \right]. \end{aligned} \quad (36)$$

In the above expression, $\Omega_r = 5.38 \times 10^{-5}$ is the radiation fraction and g_* , $g_{*,s}$ are effective degrees of freedom at horizon crossing time for each mode. Because of second order mode coupling, Ω_{GW} has quadratic dependence on scalar power spectrum $P_\zeta(k)$.

The GW fraction $\Omega_{GW}(k)$ for our hybrid model of inflation with potential in Eq. (5) is plotted in Fig. 5 against the frequency of GW given by $f_{GW} = 2\pi ck$. The top left panel in Fig. 5 for $p = 2/3$, the top right panel for linear ($p = 1$) and the middle left panel for quadratic potential ($p = 2$). The curves are drawn using the Gaussian peak function $K_g(\phi)$ (black curves) and step function $K_s(\phi)$ (blue curves). This enhancement mechanism gives rise to flatter and wider peaks in $\Omega_{GW}(k)$, which makes the primordial black hole (PBH) mass to lie in the range $\sim (10^{-15} - 1) M_\odot$. These wide peaks can be detected by SKA, NANO-Grav, LISA, Einstein Telescope and TaiJi experiments. NANO-Grav collaboration has predicted a similar broad peak in Ω_{GW} spectrum of stochastic GWs[20].

The rest of the panels (middle right, bottom left and bottom right) of Fig. 5 show three curves with different peak location and heights given in Table 3. These curves are drawn for $p = 2/3$ (middle right), $p = 1$ (bottom left) and $p = 2$ (bottom right) using the polynomial peak function $K_q(\phi)$, with $q = 2$. The blue curves on the left correspond to NG points given in Table 3 that may be the Stochastic GW wave

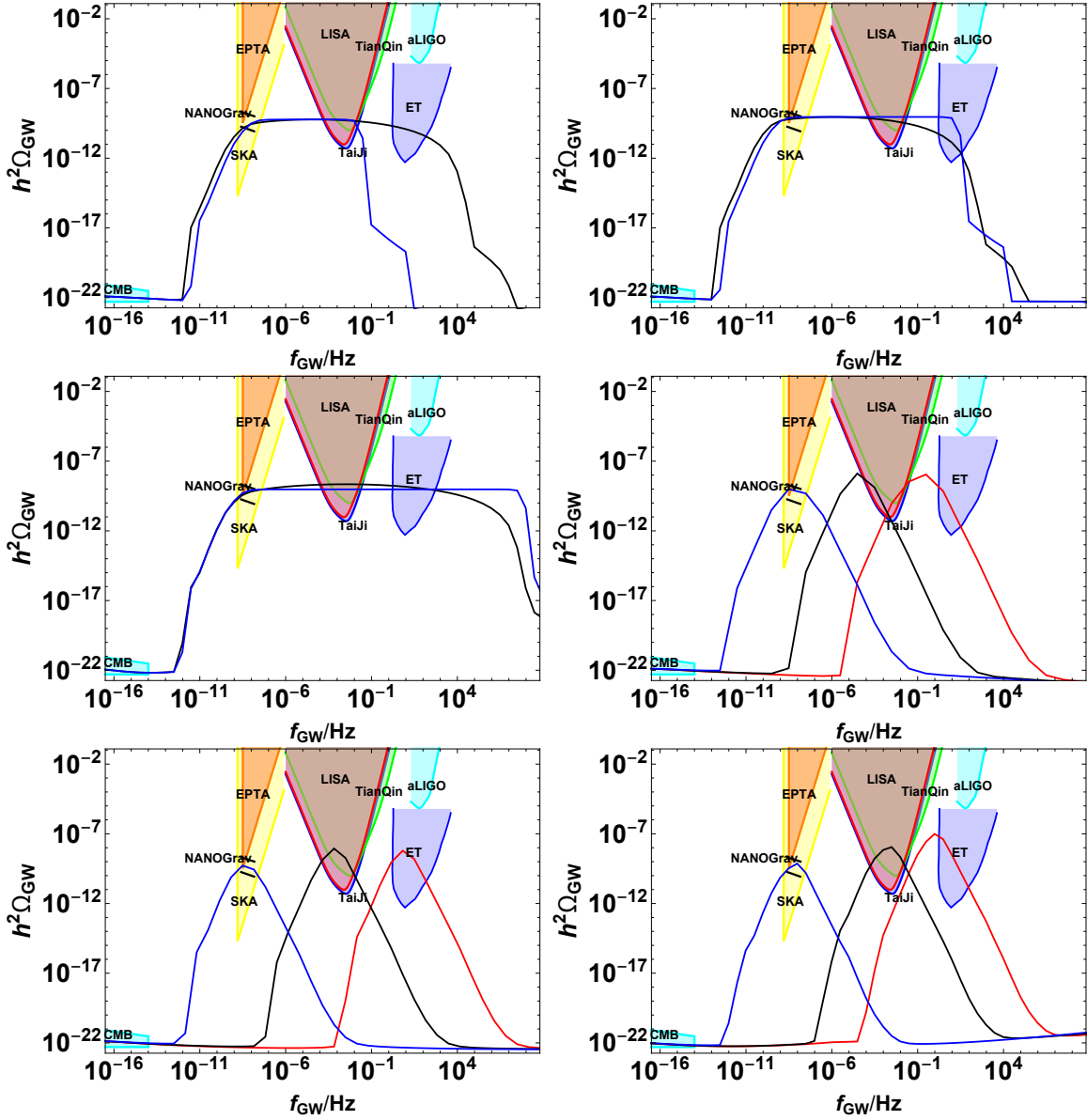


Figure 5: Gravitational wave spectra from hybrid inflation potential (5) for $p = 2/3$ (top left), $p = 1$ (top right) and $p = 2$ (middle left). The curves are drawn using Gaussian peak function $K_g(\phi)$ (black curves) and step function $K_s(\phi)$ (blue curves). The corresponding data points are given in Table 2. The remaining three panels are plotted using the polynomial peak function $K_q(\phi)$, with $q = 2$, for $p = 2/3$ (middle right), $p = 1$ (bottom left) and $p = 2$ (bottom right). The three peaks correspond to the NG (blue), TL (black) and ET (red) data points, given in Table 3.

signal detected by the NANO-Grav during its 12.5 years data release [20]. The black curves in the middle represent TL data points in Table 3 that may be detected by future space based experiments such as LISA and TaiJi. The red curves on the right

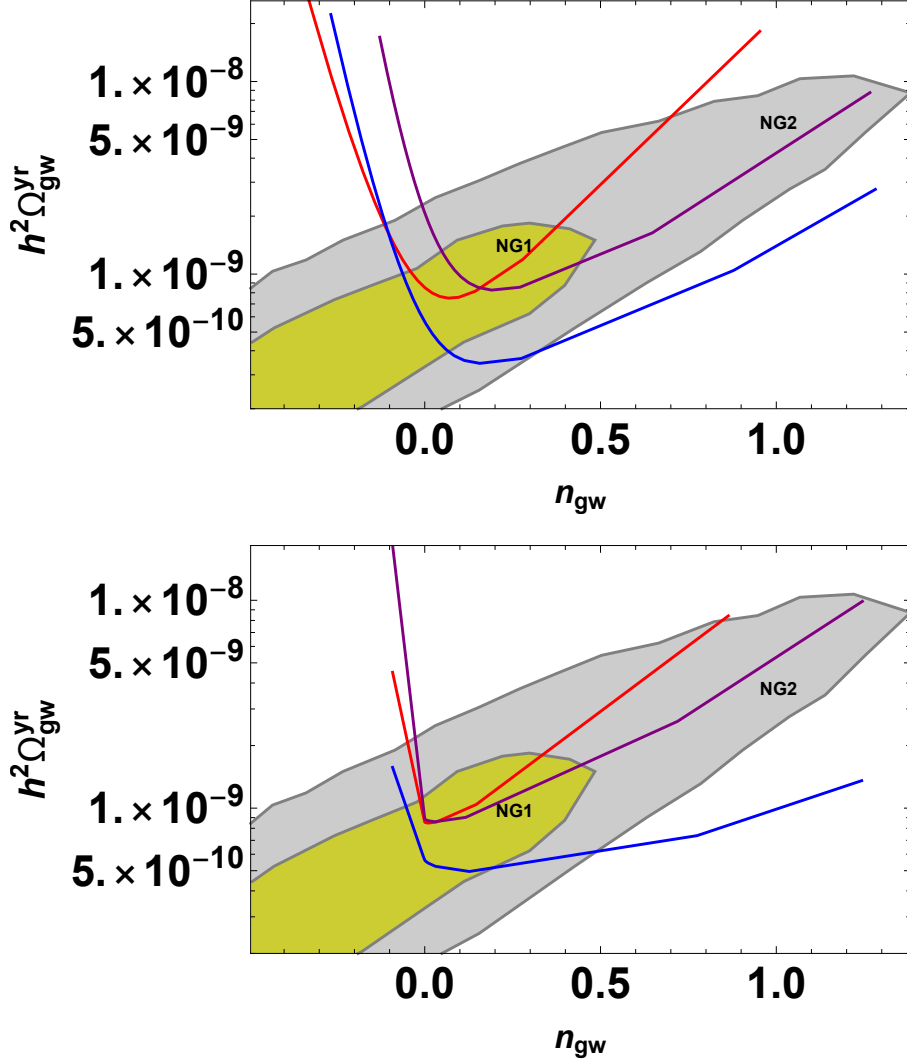


Figure 6: Gravitational wave signals from hybrid inflation compared to the NANO-Grav observations for $p = 2/3$ (blue), $p = 1$ (red) and $p = 2$ (purple). The shaded regions labeled NG1 (yellow), NG2 (grey) represent the 1- and 2-sigma regions reported by NANO-Grav [20]. The curves are drawn using enhancement mechanism of Gaussian peak function $K_g(\phi)$ (top panel) and step function $K_s(\phi)$ (bottom panel) with data points from Table 2.

represent ET data point peak that may be detected by Einstein Telescope (ET) in the future.

A fit on NANO-Grav results can be performed using the amplitude and slope of $\Omega_{GW}(f)$ from [55],

$$\Omega_{GW}(f) = \Omega_{gw}^{yr} \left(\frac{f}{f_{yr}} \right)^{n_{gw}}. \quad (38)$$

This allows direct comparison of our results to the NANO-Grav bounds in the n_{gw}

and Ω_{gw}^{yr} plane as depicted by the yellow (1-sigma) and gray (2-sigma) shaded regions in Fig. 6. We extract the amplitude and slope by comparing the amplitude at pivot scale of $f_* = 5.6 \times 10^{-9} Hz$ and taking the logarithmic derivative $\Omega_{GW}(f)$ at the pivot scale,

$$n_{gw} = \left. \frac{d \log \Omega_{GW}(f)}{d \log f} \right|_{f=f_*}, \quad (39)$$

$$\Omega_{gw}^{yr} = \Omega_{GW}(f_*) \left(\frac{f_{yr}}{f_*} \right)^{n_{gw}}. \quad (40)$$

Fig. 6 shows comparison of our predictions from hybrid inflation model (red blue and purple curves) with the constraints on the amplitude and tilt from NANO-Grav [20] (yellow and gray shaded region). The blue, red and purple curves are drawn for $p = 2/3$, $p = 1$ and $p = 2$, respectively, using Gaussian peak function $K_g(\phi)$ (top panel) and step function $K_s(\phi)$ (bottom panel.) It is quite evident from these plots that they lie within the one sigma bound of NANO-Grav. It is also important to emphasize here that the broader peaks generated by Gaussian and step peak functions give much better fitting to the NANO-Grav bounds as compared to the sharper polynomial peak functions. Moreover, the counter observations of GW by other space and ground based experiments would be considered an evidence of GUT theories of inflation and such enhancement scenarios.

6 Summary

To summarize, we have investigated Primordial Black Holes and induced Secondary Gravitational Waves using a background of Hybrid Inflation. The cosmological observables, including the tensor-to-scalar ratio r , the spectral index n_s , etc., are computed for various effective potentials. To produce the required Y_{PBH} for PBHs as a dark matter, the curvature power spectrum needs to be of the order $P_\zeta \sim 0.01$ at the scale $k > \text{Mpc}^{-1}$. To enhance the power spectrum by seven order of magnitude, we have employed a non-canonical kinetic energy term to produce primordial black hole dark matter and secondary gravitational waves. In particular, the field-dependent kinetic energy term can arise in many inflationary scenarios, such as, G-inflation, k-inflation, or general scalar-tensor theory of gravity. We have proposed three functions $K(\phi)$, with a peak at ϕ_p in order to enhance the power spectrum at small scales. The PBH mass and the frequency of secondary GWs are determined by the height h and location of ϕ_p , the peak value of power spectrum. The peak functions $K(\phi)$ induce an inflection point (with flat plateau) in the potential and effectively lead to ultra slow-roll inflation. This peak function $K(\phi)$ has a minor role away from the peak value where the usual slow-roll inflation is recovered, constrained by the CMB observations at large scales. Based on our analysis, it is quite possible that most DM constitutes PBHs if the mass of PBH DM lies within the range $(10^{-16} - 10^{-11}) M_\odot$.

and $(1 - 10) M_{\odot}$. The enhanced power spectra of primordial curvature perturbations can have both sharp and broad peaks. Large mass range of PBH is realized in mechanisms used above which produce PBHs of different masses, ranging from $(10^{-16} - 10) M_{\odot}$. The frequencies of SIGWs range from nHz to kHz, which can be detected in future space-based GW observatories like LISA, TaiJi, EPTA, SKA, ET, and TianQin. The SIGWs associated with the formation of solar mass PBH can be interpreted as the stochastic GW signal detected by NANO-Grav. The broad peaks in $\Omega_{GW}(f)$ from Gaussian and step peaks in nHz range fit well with the signal detected by the NANO-Grav.

Acknowledgments

The authors would especially like to thank George K. Leontaris for very useful discussions, comments and revising the draft.

References

- [1] G. Bertone and D. Hooper, Rev. Mod. Phys. **90**, no.4, 045002 (2018) doi:10.1103/RevModPhys.90.045002 [arXiv:1605.04909 [astro-ph.CO]].
- [2] Y. B. Zel'dovich and I. D. Novikov, The Hypothesis of Cores Retarded during Expansion and the Hot Cosmological Model, Sov. Astron. **10**, 602 (1967).
- [3] S. Hawking, Gravitationally collapsed objects of very low mass, Mon. Not. Roy. Astron. Soc. **152**, 75 (1971).
- [4] B. J. Carr and S. W. Hawking, Black holes in the early Universe, Mon. Not. Roy. Astron. Soc. **168**, 399 (1974).
- [5] M. Y. Khlopov, Primordial Black Holes, Res. Astron. Astrophys. **10**, 495 (2010) [arXiv:0801.0116 [astro-ph]].
- [6] M. Sasaki, T. Suyama, T. Tanaka and S. Yokoyama, Primordial black holes – perspectives in gravitational wave astronomy, Class. Quant. Grav. **35**, no. 6, 063001 (2018) [arXiv:1801.05235 [astro-ph.CO]].
- [7] B. Carr, F. Kuhnel and M. Sandstad, Primordial Black Holes as Dark Matter, Phys. Rev. D **94**, no. 8, 083504 (2016) [arXiv:1607.06077 [astro-ph.CO]].
- [8] B. Carr and F. Kuhnel, Primordial black holes with multimodal mass spectra, Phys. Rev. D **99**, no. 10, 103535 (2019) [arXiv:1811.06532 [astro-ph.CO]].
- [9] S. W. Hawking, Black hole explosions, Nature **248**, 30 (1974).

- [10] J. H. MacGibbon and B. J. Carr, Cosmic rays from primordial black holes, *Astrophys. J.* **371**, 447 (1991).
- [11] B. J. Carr, K. Kohri, Y. Sendouda and J. Yokoyama, New cosmological constraints on primordial black holes, *Phys. Rev. D* **81**, 104019 (2010) [arXiv:0912.5297 [astro-ph.CO]].
- [12] H. Niikura, M. Takada, S. Yokoyama, T. Sumi and S. Masaki, Constraints on Earth-mass primordial black holes from OGLE 5-year microlensing events, *Phys. Rev. D* **99**, no. 8, 083503 (2019) [arXiv:1901.07120 [astro-ph.CO]].
- [13] B. J. Carr and M. Sakellariadou, Dynamical constraints on dark compact objects, *Astrophys. J.* **516**, 195 (1999).
- [14] C. M. Deng, Y. Cai, X. F. Wu and E. W. Liang, Fast Radio Bursts From Primordial Black Hole Binaries Coalescence, *Phys. Rev. D* **98**, no. 12, 123016 (2018) [arXiv:1812.00113 [astro-ph.HE]].
- [15] B. P. Abbott *et al.* (LIGO Scientific Collaboration and Virgo Collaboration), *Phys. Rev. Lett.* **116**, 061102 (2016).
- [16] B. P. Abbott *et al.* (LIGO Scientific Collaboration and Virgo Collaboration), *Phys. Rev. Lett.* **116**, 241103 (2016).
- [17] B. P. Abbott *et al.* (LIGO Scientific Collaboration and Virgo Collaboration), *Phys. Rev. Lett.* **118**, 221101 (2017).
- [18] B. P. Abbott *et al.* (LIGO Scientific Collaboration and Virgo Collaboration), *Astrophys. J.* **851**, L35 (2017).
- [19] B. P. Abbott *et al.* (LIGO Scientific Collaboration and Virgo Collaboration), *Phys. Rev. Lett.* **119**, 141101 (2017).
- [20] Z. Arzoumanian *et al.* [NANO-Grav], *Astrophys. J. Lett.* **905**, no.2, L34 (2020) doi:10.3847/2041-8213/abd401 [arXiv:2009.04496 [astro-ph.HE]].
- [21] M. Sasaki, T. Suyama, T. Tanaka and S. Yokoyama, Primordial Black Hole Scenario for the Gravitational-Wave Event GW150914, *Phys. Rev. Lett.* **117**, no. 6, 061101 (2016) Erratum: [*Phys. Rev. Lett.* **121**, no. 5, 059901 (2018)] [arXiv:1603.08338 [astro-ph.CO]].
- [22] V. Mandic, S. Bird and I. Cholis, Stochastic Gravitational-Wave Background due to Primordial Binary Black Hole Mergers, *Phys. Rev. Lett.* **117**, no. 20, 201102 (2016) [arXiv:1608.06699 [astro-ph.CO]].

- [23] S. Wang, Y. F. Wang, Q. G. Huang and T. G. F. Li, Constraints on the Primordial Black Hole Abundance from the First Advanced LIGO Observation Run Using the Stochastic Gravitational-Wave Background, *Phys. Rev. Lett.* **120**, no. 19, 191102 (2018) [arXiv:1610.08725 [astro-ph.CO]].
- [24] D. Baumann, P. J. Steinhardt, K. Takahashi and K. Ichiki, *Phys. Rev. D* **76**, 084019 (2007) doi:10.1103/PhysRevD.76.084019 [arXiv:hep-th/0703290 [hep-th]].
- [25] K. N. Ananda, C. Clarkson and D. Wands, *Phys. Rev. D* **75**, 123518 (2007) [arXiv:gr-qc/0612013 [gr-qc]].
- [26] K. Kohri and T. Terada, Semianalytic calculation of gravitational wave spectrum nonlinearly induced from primordial curvature perturbations, *Phys. Rev. D* **97**, no. 12, 123532 (2018) [arXiv:1804.08577 [gr-qc]].
- [27] N. Bartolo, V. De Luca, G. Franciolini, M. Peloso, D. Racco and A. Riotto, Testing primordial black holes as dark matter with LISA, *Phys. Rev. D* **99**, no. 10, 103521 (2019) [arXiv:1810.12224 [astro-ph.CO]].
- [28] Y. F. Cai, C. Chen, X. Tong, D. G. Wang and S. F. Yan, When Primordial Black Holes from Sound Speed Resonance Meet a Stochastic Background of Gravitational Waves, *Phys. Rev. D* **100**, no. 4, 043518 (2019) [arXiv:1902.08187 [astro-ph.CO]].
- [29] R. g. Cai, S. Pi and M. Sasaki, Gravitational Waves Induced by non-Gaussian Scalar Perturbations, *Phys. Rev. Lett.* **122**, no. 20, 201101 (2019) [arXiv:1810.11000 [astro-ph.CO]].
- [30] V. De Luca, G. Franciolini and A. Riotto, *Phys. Rev. Lett.* **126**, no.4, 041303 (2021) [arXiv:2009.08268 [astro-ph.CO]]. K. Inomata, M. Kawasaki, K. Mukaida and T. T. Yanagida, *Phys. Rev. Lett.* **126**, no.13, 131301 (2021) [arXiv:2011.01270 [astro-ph.CO]]. V. Vaskonen and H. Veermäe, *Phys. Rev. Lett.* **126**, no.5, 051303 (2021) [arXiv:2009.07832 [astro-ph.CO]].
- [31] Y. Akrami *et al.* [Planck], *Astron. Astrophys.* **641**, A10 (2020) [arXiv:1807.06211 [astro-ph.CO]].
- [32] J. Lin, Q. Gao, Y. Gong, Y. Lu, C. Zhang and F. Zhang, *Phys. Rev. D* **101**, no.10, 103515 (2020) [arXiv:2001.05909 [gr-qc]].
- [33] Y. Lu, Y. Gong, Z. Yi and F. Zhang, *JCAP* **12**, 031 (2019) [arXiv:1907.11896 [gr-qc]].
- [34] J. Garcia-Bellido, M. Peloso and C. Unal, *JCAP* **09**, 013 (2017) doi:10.1088/1475-7516/2017/09/013 [arXiv:1707.02441 [astro-ph.CO]].

- [35] S. Matarrese, S. Mollerach and M. Bruni, Phys. Rev. D **58**, 043504 (1998) [arXiv:astro-ph/9707278 [astro-ph]].
- [36] R. D. Ferdman, R. van Haasteren, C. G. Bassa, M. Burgay, I. Cognard, A. Corongiu, N. D’Amico, G. Desvignes, J. W. T. Hessels and G. H. Janssen, *et al.* Class. Quant. Grav. **27**, 084014 (2010) doi:10.1088/0264-9381/27/8/084014 [arXiv:1003.3405 [astro-ph.HE]]. G. Hobbs, A. Archibald, Z. Arzoumanian, D. Backer, M. Bailes, N. D. R. Bhat, M. Burgay, S. Burke-Spolaor, D. Champion and I. Cognard, *et al.* Class. Quant. Grav. **27**, 084013 (2010) doi:10.1088/0264-9381/27/8/084013 [arXiv:0911.5206 [astro-ph.SR]]. M. A. McLaughlin, Class. Quant. Grav. **30**, 224008 (2013) doi:10.1088/0264-9381/30/22/224008 [arXiv:1310.0758 [astro-ph.IM]]. G. Hobbs, Class. Quant. Grav. **30**, 224007 (2013) doi:10.1088/0264-9381/30/22/224007 [arXiv:1307.2629 [astro-ph.IM]]. K. Danzmann, Class. Quant. Grav. **14**, 1399-1404 (1997) doi:10.1088/0264-9381/14/6/002
- [37] P. Amaro-Seoane *et al.* [LISA], [arXiv:1702.00786 [astro-ph.IM]].
- [38] W. R. Hu and Y. L. Wu, Natl. Sci. Rev. **4**, no.5, 685-686 (2017) doi:10.1093/nsr/nwx116
- [39] J. Luo *et al.* [TianQin], Class. Quant. Grav. **33**, no.3, 035010 (2016) doi:10.1088/0264-9381/33/3/035010 [arXiv:1512.02076 [astro-ph.IM]].
- [40] W. Ahmed, O. Ishaque and M. U. Rehman, Int. J. Mod. Phys. D **25**, no.03, 1650035 (2016) doi:10.1142/S0218271816500358 [arXiv:1501.00173 [hep-ph]].
- [41] S. R. Coleman and E. J. Weinberg, “Radiative Corrections as the Origin of Spontaneous Symmetry Breaking,” Phys. Rev. D **7**, 1888 (1973).
- [42] V. N. Senoguz and Q. Shafi, “Chaotic inflation, radiative corrections and precision cosmology,” Phys. Lett. B **668**, 6 (2008) [arXiv:0806.2798 [hep-ph]].
- [43] G. R. Dvali, Q. Shafi and R. K. Schaefer, “Large scale structure and supersymmetric inflation without fine tuning,” Phys. Rev. Lett. **73**, 1886 (1994) [arXiv:hep-ph/9406319].
- [44] T. Kobayashi, M. Yamaguchi and J. Yokoyama, Phys. Rev. Lett. **105**, 231302 (2010) [arXiv:1008.0603 [hep-th]].
- [45] J. Garriga and V. F. Mukhanov, Phys. Lett. B **458**, 219-225 (1999) [arXiv:hep-th/9904176 [hep-th]].
- [46] D. Baumann, TASI Lectures on Primordial Cosmology, [arXiv:1807.03098 [hep-th]].

- [47] Jennifer A. Adams, Graham G. Ross and Subir Sarkar, Phys. Lett. B 391 (1997) 271-280, [arXiv: 9608336 [hep-ph]]. Jennifer Adams, Bevan Cresswell and Richard Easther, Phys.Rev.D 64 (2001) 123514, [arXiv: 0102236 [astro-ph]].
- [48] B. J. Carr, Astrophys. J. **201**, 1-19 (1975) doi:10.1086/153853
- [49] O. Özsoy, S. Parameswaran, G. Tasinato and I. Zavala, JCAP **07**, 005 (2018) doi:10.1088/1475-7516/2018/07/005 [arXiv:1803.07626 [hep-th]].
- [50] Y. Tada and S. Yokoyama, Phys. Rev. D **100**, no.2, 023537 (2019) doi:10.1103/PhysRevD.100.023537 [arXiv:1904.10298 [astro-ph.CO]].
- [51] N. Aghanim *et al.* [Planck], Astron. Astrophys. **641**, A6 (2020) doi:10.1051/0004-6361/201833910 [arXiv:1807.06209 [astro-ph.CO]].
- [52] I. Musco and J. C. Miller, Class. Quant. Grav. **30**, 145009 (2013) doi:10.1088/0264-9381/30/14/145009 [arXiv:1201.2379 [gr-qc]].
- [53] Bardeen, J. M. (1980) Gauge-invariant cosmological perturbations, Phys. Rev. D 22, 1882-1905.
- [54] K. Inomata and T. Terada, Phys. Rev. D101, 023523 (2020), arXiv:1912.00785 [gr-qc].
- [55] Wilfried Buchmuller, Valerie Domcke and Kai Schmitz, Phys.Lett.B 811 (2020) 135914, [arXiv:1201.2379 [gr-qc]].